Crystallization Properties of the $Ge_2Sb_2Te_5$ Phase-Change Compound from Advanced Simulations

*Ider Ronneberger, Wei Zhang, Hagai Eshet, and Riccardo Mazzarello**

$Ge_2Sb_2Te_5$ (GST) is an important phase-change material used in optical and electronic memory devices. In this work, crystal growth of GST at 600 K is investigated by ab initio molecular dynamics. Simulations of two different crystallization processes are performed. In the first set of simulations, the growth of crystalline nuclei generated using the metadynamics method is studied. In the second set, models containing a planar amorphous–crystalline interface are considered and the crystallization at the interface is investigated. The extracted crystal growth velocities are in the range of 1 m s^{-1} in both cases and compare well with recent experimental measurements. It is also found that GST crystallizes into a disordered cubic phase in all the simulations.

1. Introduction

Optical storage devices and electronic memories based on phase-change materials (PCMs) exploit the optical and electronic contrast displayed by their crystalline and amorphous phase.[1–3] In these devices, high-speed switching stems from the ability of PCMs to undergo fast transitions (induced by optical or electrical pulses) between the two states, whereas long retention times originate from the remarkable thermal stability of both phases at room temperature. The extremely strong dependence of the crystallization speed on temperature has recently been linked to the high fragility of PCMs.[4–10] More specifically, this behavior has been attributed to a pronounced change in the activation energy and the prefactor for growth velocity as a function of temperature, which is a fingerprint of fragility.

The GeSbTe compounds lying on the pseudobinary line $GeTe–Sb_2Te_3$ are the most widely studied family of PCMs, due to their applications in DVD-RAM, rewritable Blu-Ray discs, and phase-change memories.[11–21] Recrystallization of GST is known to be triggered by nucleation events. However, in state-of-the-art memory cells, it may be governed by crystal growth at the interface with the crystalline matrix, due to the small size of the amorphous mark. For system sizes of the order of nanometers, crystallization occurs on the sub-nanosecond time scale at elevated temperatures, opening up the possibility of investigating this phenomenon by ab initio molecular dynamics (AIMD) based on density functional theory (DFT).[22–26] In previous studies[22–24] amorphous models of the prototypical compound $Ge_2Sb_2Te_5$ (GST) containing 60–180 atoms were crystallized using AIMD. These works provided valuable information about the microscopic mechanisms of crystallization, although they did not assess finite size effects, which are expected to play an important role in such small samples. Larger models of GST containing 460 and 640 atoms were later studied:[25,26] in one study,[25] crystallization was facilitated by inserting a crystalline seed inside the amorphous network, whereas, in another[26] extremely long simulations (4 ns) of 460-atoms models without structural constraints were carried out.

The stable crystalline phase of GST is hexagonal and consists of alternating Ge, Sb, and Te layers.[27] However, there is experimental evidence that, upon fast crystallization of the glass or the supercooled liquid, a metastable rocksalt phase is formed. In this phase, Te atoms occupy one face-centered cubic sublattice, whereas Ge, Sb, and vacancies are randomly arranged in the second one. The amount of disorder in this sublattice is difficult to ascertain. Recently, it has been shown experimentally,[28] and subsequently corroborated by theory,[29] that the degree of randomness in crystalline GeSbTe and similar compounds (such as $Ge_1Sb_2Te_4$) can be reduced by thermal annealing, so as to induce disorder-driven insulator–metal transitions.

In this work, we carry out AIMD simulations to study the crystallization kinetics of GST at high temperature (≈600 K) and estimate its growth velocity, as well as to determine the structural properties of the recrystallized phase, including the layer stacking

I. Ronneberger, Dr. W. Zhang, Prof. R. Mazzarello
Institute for Theoretical Solid State Physics
RWTH Aachen University
52056 Aachen, Germany
E-mail: mazzarello@physik.rwth-aachen.de
Dr. W. Zhang
I. Institute of Physics (IA)
RWTH Aachen University
52056 Aachen, Germany
Dr. H. Eshet
Department of Chemistry and Applied Biosciences and
Facoltà di Informatica
ETH Zurich and Università della Svizzera Italiana
6900 Lugano, Switzerland
Dr. H. Eshet
School of Chemistry
The Sackler Faculty of Exact Sciences
Tel Aviv University
Tel Aviv 69978, Israel
Prof. R. Mazzarello
JARA-FIT and JARA-HPC
RWTH Aachen University
52056 Aachen, Germany

DOI: 10.1002/adfm.201500849

© 2015 WILEY-VCH Verlag GmbH & Co. KGaA, Weinheim

sequence and the amount of disorder. We consider two sets of simulations. In the first one, we use metadynamics, an enhanced sampling method,[30] to accelerate the formation of sizable crystallites and then we let the nuclei grow by performing standard "unbiased" AIMD simulations. In the second set, we consider amorphous models inside a crystalline matrix, obtained by fixing two atomic layers at the crystalline positions during melting and subsequent quenching. The latter simulations describe crystallization of very small amorphous marks (wherein the probability of forming critical crystalline nuclei is low), as well as growth at the boundary of large nuclei. We thoroughly compare the crystal growth velocities and the structural properties of the recrystallized models obtained from the two sets of simulations.

2. Methods

The models are heated at 3000 K and then cooled down to the melting temperature, at which they are equilibrated for 30 ps. The amorphous state is obtained by quenching down to 300 K, with a quenching rate of 10^{13} K s^{-1}. The models are then equilibrated at this temperature for another 30 ps. To study the crystallization behavior, we increase the temperature to 600 K and perform canonical simulations, after 25 ps equilibration. We consider purely amorphous models containing 460 atoms in a cubic 2.44 nm × 2.44 nm × 2.44 nm supercell (first set) and 540-atom models in an elongated orthorhombic 2.25 nm × 2.16 nm × 3.51 nm cell containing a crystalline matrix (second set). We employ the "second-generation" Car–Parrinello scheme[31] implemented in the Quickstep code of the CP2K package.[32] In this code, periodic boundary conditions are enforced. We use the generalized gradient approximation (GGA) to the exchange-correlation potential[33] and scalar-relativistic Goedecker pseudopotentials.[34] The Kohn–Sham orbitals are expanded in a triple-zeta plus polarization Gaussian-type basis set, whereas the charge density is expanded in plane waves with a cutoff of 300 Ry. The Brillouin zone is sampled at the Γ point of the supercell. The time step for the simulations is 2 fs. The density is fixed at a value (0.0317 $Å^{-3}$) lying between the experimental amorphous value (0.0300 $Å^{-3}$) and the crystalline one (0.0328 $Å^{-3}$). Simulations at fixed density are relevant to phase-change memory cells, wherein the presence of a crystalline matrix constrains the volume available during recrystallization of the amorphous mark.

Metadynamics is an enhanced sampling technique that enables an efficient exploration of the phase space and allows one to estimate the free energy changes in a molecular dynamics simulation.[30] The method is based on the assumption that the process of interest can be characterized by a (small) set of collective variables (CVs) $\{\xi_i\}_i = 1, d$, which are functions of the atomic coordinates and describe the relevant degrees of freedom of the system. A history-dependent biasing potential V_G is added to the potential energy of the system during the MD run. V_G is a sum of Gaussians in the d-dimensional space of the CVs. The Gaussians are centered at values ξ_i^s taken at the time intervals $\tau, 2\tau, 3\tau, \ldots, < t$

$$V_G\left(\{\xi_i\}_{i=1,d}, t\right) = w \sum_{s=\tau,2\tau,<t} \exp\left(-\sum_{i=1}^{d} \frac{\left(\xi_i - \xi_i^s\right)^2}{2\sigma_i}\right) \quad (1)$$

w and σ_i are the height and width of the Gaussians, which determine the accuracy and the efficiency of the simulation.

3. Results

3.1. Growth of Crystalline Nuclei Generated Using Metadynamics

To create crystalline nuclei in the first set of models, we exploit the ability of metadynamics to accelerate rare events by biasing the system and exploring the phase space along the chosen CVs.[30] We employ the potential energy U and the bond order correlation parameter "dot-product" q_4^{dot},[35] averaged over a set of atoms within a predefined sphere, as CVs. Similar variables have been used in previous classical molecular dynamics studies of crystallization.[36] The use of a local CV enables us to preselect the region where the nucleus will form during the metadynamics simulation (although, in principle, crystallites may also form outside this region). It also helps to reduce spurious effects due to the periodic boundary conditions by favoring the formation of quasi-spherical nuclei. Further information about the simulation parameters is provided in the Supporting Information.

We succeed in generating several independent models containing large crystalline clusters, consisting of 100–150 particles, which serve as a starting point for further unbiased growth simulations, three of which lead to crystallization of the models. These trajectories are used to calculate the growth velocity. Typical timescales for the generation of said nuclei are of the order of 100 ps. Unbiased simulations would require much longer simulation times to observe the stochastic formation of large (post-critical) nuclei. We do not determine the size of critical nuclei nor the energy barriers for nucleation: this is beyond the scope of this work.

In **Figure 1**, we show some snapshots of the crystallization process of one of the models. The first snapshot corresponds to the starting time of the unbiased simulation. The three models start to grow from a quasi-spherical nucleus in all directions before meeting their periodic images along one or two directions. At the end of the growth process, relatively small noncrystalline regions can still be observed. Complete crystallization is not possible due to mismatch effects. We also use the q_4^{dot} variable to distinguish between crystalline-like and amorphous-like particles during crystal growth. To estimate the growth velocity v_g, we compute the total volume of the crystalline part V_c at each time step by summing up the volumes of the Voronoi polyhedra[37] around the crystalline-like atoms, as well as the total area of the interface between the amorphous and the crystalline phase (see Supporting Information). In **Figure 2**, the volume of the crystalline part and the growth velocity as a function of time are displayed. We obtain a growth velocity of 1.2 m s^{-1} by averaging over time and three models.

3.2. Growth from a Planar Amorphous–Crystalline Interface

In order to gain a better understanding of the microscopic crystallization mechanisms, we also consider a set of models

© 2015 WILEY-VCH Verlag GmbH & Co. KGaA, Weinheim

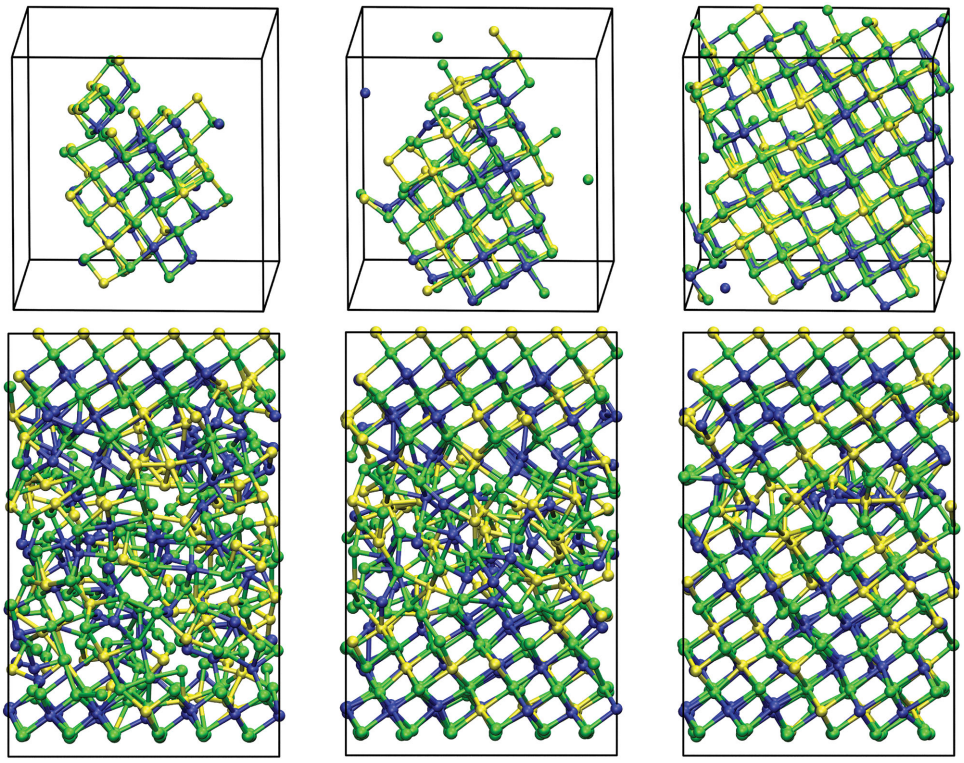

Figure 1. Snapshots of the crystallization process of a 460-atom model containing a crystalline nucleus generated using metadynamics (upper panel) and of a 540-atom model containing a planar crystal–amorphous interface (lower panel). In the upper panels, only crystalline-like atoms (corresponding to $q_4^{dot} > 0.45$) are shown. Te atoms are green, Sb atoms are yellow, and Ge atoms are blue.

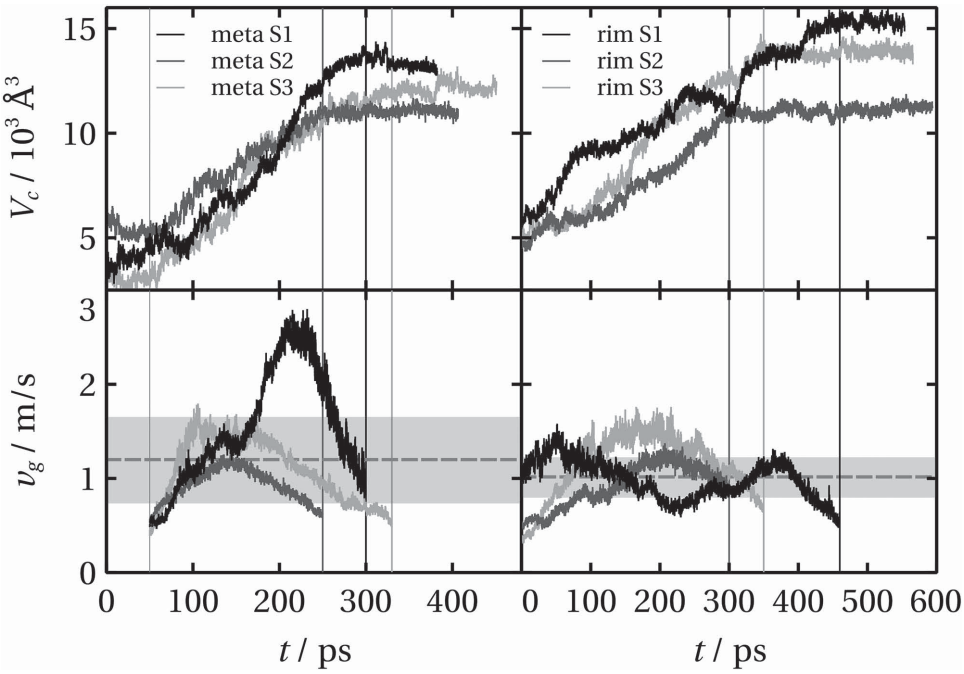

Figure 2. Volume of the crystalline region V_c and crystal growth velocity v_g as a function of time for all the six models. The first and second sets of models are denoted with "meta" and "rim," respectively. Each set consists of three independent trajectories S1, S2, and S3. The growth velocities are calculated within the time windows indicated with thin lines. The average velocity and the standard deviation for each of the two sets are indicated with a dashed line and a shaded area.

© 2015 WILEY-VCH Verlag GmbH & Co. KGaA, Weinheim

containing a simple planar amorphous–crystalline interface. Simulations of amorphous models inside a crystalline matrix have been recently carried out to study crystallization of GeTe[9] and Ag, In-doped Sb_2Te (AIST).[10] Here, we investigate crystal growth along the [111] direction of the cubic lattice, corresponding to the [0001] direction of the hexagonal phase, and we carry out three independent simulations of crystallization. The cell size along [111] is such that it can contain 20 crystalline layers. Hence, the supercell can fully accommodate the hexagonal phase (where two layers out of 20 are "vacancy layers")[27,29] but not the cubic rocksalt phase, which requires the number of layers being a multiple of 6. Moreover, the two layers we fix during melting and quenching are disorder-free and consist of Te and Sb atoms, respectively. In spite of this, all the three models crystallize into the cubic phase (as shown in the Supplementary Information), although, due to the mismatch, they do not crystallize completely. This finding is in line with previous experiments on crystallization of amorphous GST thin films on the top of cubic and hexagonal crystalline GST.[38] In these experiments, crystallization was shown to proceed mainly from the amorphous–crystalline interface and the recrystallized region near the interface was always found to be in the cubic phase, irrespective of the stacking of the underlying crystal.

First, we check whether the trajectories exhibit nucleation events. For this purpose, we monitor the evolution of q_4^{dot} for each atom. No such event is observed. This leads to the important conclusion that, for such small sizes of the amorphous mark, crystallization of GST is dominated by growth from the rim. Figure 1 displays some snapshots of the crystallization trajectory of one of the models. To elucidate the properties of the amorphous–crystalline interface, we divide the supercell into slabs along the direction of growth (assumed to be parallel to z) and calculate the profiles of Q_4^{dot} (where Q_4^{dot} denotes the average of q_4^{dot} over a set of atoms) and of the D coefficients along z, D_z. **Figure 3** shows the Q_4^{dot} and D_z profiles, averaged over the three samples. The interface is the region where Q_4^{dot} increases from ≈0.1 (glass) to the ≈0.9 (crystal) (see also the Supplementary Information). It extends over two to four layers (5–7 Å). The profiles of D_z turn out to be as sharp as those of Q_4^{dot}, as occurs in AIST.[10] The relatively strong fluctuations of D_z in the amorphous region are due to poor averaging, i.e., to the small number of particles in each slab. The value of D_z averaged over all the slabs in the amorphous region compares well with the bulk value (1.6×10^{-10} m^2 s^{-1}), which we obtained from independent calculations of the mean squared displacements (on a 80 ps time scale) in a completely amorphous model of GST.

Having assessed that crystal growth occurs solely at the interface, we can extract v_g from the trajectories. The growth velocity is estimated in the same manner as for the first set of models. The corresponding average value of v_g is of the order of 1 m s^{-1} (see Figure 2). Hence, the two sets of simulations yield growth velocity values in very good agreement with each other. We also check the results using a more straightforward approach, wherein v_g is computed from the ratio $LN_c(t)/(2Nt)$, where $N_c(t)$ and N are the number of crystalline-like particles at time t and the total number of particles, respectively, and L is the length (along the growth direction) of a supercell which accommodates a fully crystallized model of cubic GST. The

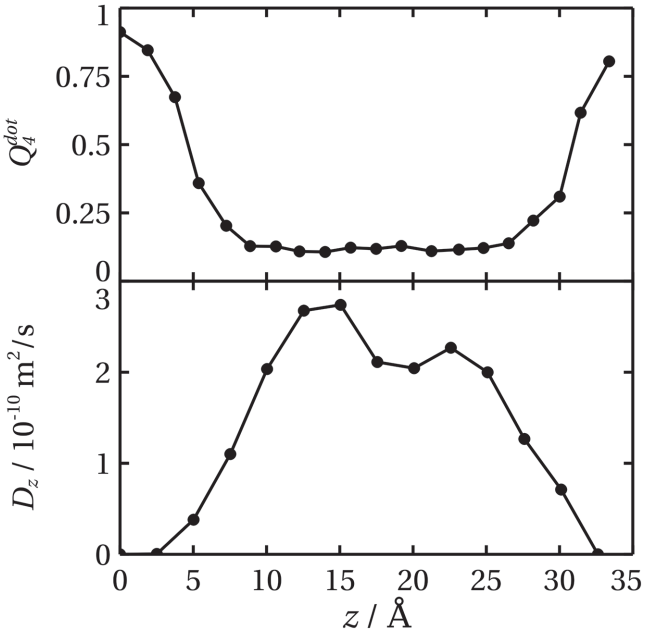

Figure 3. Profile of Q_4^{dot} (upper panel) and of the diffusion coefficient D_z (lower panel) along the direction of growth z for the second set of models at the initial stages of the crystallization process. The profile of D_z is derived from the mean-square displacements in the z-direction, which are calculated by averaging over the atoms in each slab and over time (50 ps). The two profiles are obtained by averaging over the three models.

second approach yields an average growth velocity of 1.4 m s^{-1}. The deviation stems from the fact that the Voronoi method gives larger interface areas and thus lower velocities.

We also compute the deposition rate k^+, defined as the rate at which atoms impinge on the interface, and the sticking coefficient S, defined as the probability for an atom impinging on the interface to become part of the crystal. k^+ is given by the number of "impinging events" per unit time, whereas the sticking coefficient is computed as $S = (n_i - n_e)/n_i$, where n_i and n_e indicate the total number of impinging and escaping events, respectively. v_g is proportional to the product of k^+ and S: $v_g = \lambda k^+ \cdot S$, where λ is a length of the order of the diffusional jump distance. To compute these quantities, we use the same method as in ref. [10]. The values of k^+ and S calculated by averaging over the three trajectories are 0.05 ps^{-1} and 0.21, respectively. Such large values explain the high growth velocity of GST. High deposition rates stem from the large bulk diffusion coefficients (1.6×10^{-10} m^2 s^{-1}) and the presence of a thin amorphous–crystalline interface. The large sticking coefficients are instead due to the pronounced supercooling and the consequent large driving force (i.e., the large difference between the chemical potential of the crystalline and amorphous state).

Although fast, the growth velocity of GST is almost one order of magnitude lower than that of AIST at similar temperature.[10] The reason for this behavior is twofold: a) the atomic diffusivities in GST are smaller than in AIST (1.6×10^{-10} m^2 s^{-1} vs 4.9×10^{-10} m^2 s^{-1})[10] and b) the sticking coefficients of GST are also smaller with respect to AIST (0.2 vs 0.38).[10] The latter point may be related to the fact that AIST crystallizes into an extremely disordered phase, wherein all the layers are

© 2015 WILEY-VCH Verlag GmbH & Co. KGaA, Weinheim

characterized by a large amount of compositional Sb/Te disorder. On the other hand, recrystallized GST consists of alternating cation Ge/Sb layers and anion Te layers: the former contain randomly arranged Ge and Sb atoms and vacancies, whereas the latter exhibit small chemical disorder (see the next section).

3.3. Structural Properties of the Amorphous and Recrystallized Phase

The recrystallized cubic models contain a large number of defects, which include vacancies and compositional disorder. As regards the latter, we do not only observe a random distribution of Ge and Sb atoms on the cation sublattice but also a small fraction (of order 3%) of antisite Te defects (i.e., Te atoms at Ge/Sb sublattice sites), in agreement with previous simulations.[25,26] As a consequence, some Te–Te bonds are also present in our models.

In recent DFT work,[29] we have shown that, in strongly disordered cubic GST, the presence of vacancy clusters (i.e., regions having a vacancy concentration much higher than the average value) leads to the formation of localized electronic states at the Fermi level E_F and, thus, insulating behavior. Vacancy clusters are energetically unfavorable;[29] however, it is plausible that they form during rapid crystallization of the amorphous phase. Although the present models of GST are too small to directly observe electron localization at E_F, it is interesting to analyze the distribution of vacancies in these models to assess whether vacancy clusters are indeed present after crystallization. It is also useful to study the arrangement of cavities in the amorphous phase and their evolution along the crystallization trajectories to shed light on the role they play during the growth process.[24,25]

We use the Voronoi S-network generated by the VNP code[39] to compute the concentration of voids and their distribution in both crystalline and amorphous states. Such an approach is well suited to the analysis of the structurally complex amorphous network. We employ a probe sphere size of R_p = 1.3 Å. The distribution of cavities for two models, before and after crystallization, is shown in **Figure 4**. We define the cavity volumes to be simple Delaunay simplices, as discussed in the Supporting Information. Because of the different definitions and set of parameters, the absolute values obtained for the cavity volumes cannot be directly compared with the results from previous studies.[18,25] The total volume of the cavities takes values of 4%–6% in the initial amorphous models containing a crystalline layer or nucleus. The cavity size distribution shows a broad range of small (V < 25 Å^3) and large (V > 30 Å^3) cavities and a peak in the range of 25–30 Å^3 corresponding to the size of a

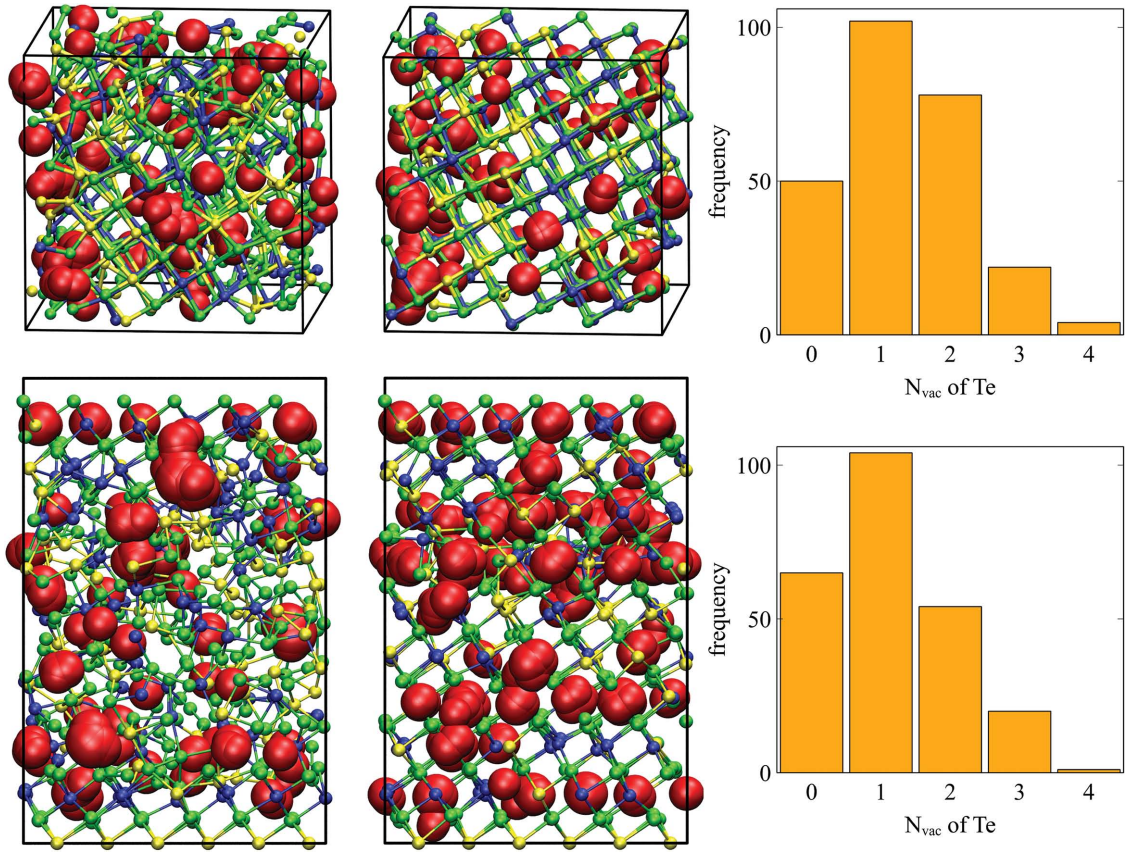

Figure 4. Cavity and vacancy distribution at the initial (left panels) and final (middle panels) stages of crystallization for a model of set 1 (upper panels) and 2 (lower panels). The right panels show histograms of the number of nearest neighbor vacancies N_{vac} of the Te atoms in the two recrystallized models.

© 2015 WILEY-VCH Verlag GmbH & Co. KGaA, Weinheim

single vacancy. The total cavity volume increases linearly during the crystallization and the final values are 6%–9%, depending on the degree of crystallization. Notice again that the final crystalline structures in both simulation sets contain small disordered regions, which cannot crystallize due to mismatch effects. The increase in the total cavity volume upon crystallization might stem from the fact that the volume of the cell was fixed during the simulations.

The localized wave functions near E_F of insulating models of crystalline GST have been shown to consist mainly of the p orbitals of Te atoms with 3 (Te^{3v}) and 4 (Te^{4v}) nearest neighbor vacancies.[29] Both configurations are present in our recrystallized models, as shown in Figure 4. In particular, the amount of Te^{3v} atoms is quite significant, of order 6%. We also find that configurations containing vacancies on opposite sides of a Te atom are relatively rare: in the case of Te atoms with two and three neighboring vacancies, the occurrence of such configurations is about 4% and 8%, respectively. In summary, both sets of simulations indicate that, in the recrystallized models, vacancies are randomly distributed on one sublattice and form a few large clusters (see the Supplementary Information). It is important to stress that further annealing of the recrystallized models at 600 K on longer time scales (currently not accessible by AIMD simulations) should lead to the ordering of vacancies and to the transition to the hexagonal phase.[28] In agreement with refs. [25,26], we do not observe the formation of vacancy-free crystallites, which was previously reported.[24]

4. Discussion and Conclusions

The growth velocity of GST was also estimated to be of the order of 1 m s^{-1} at 600 K in the literature.[26] Since, in the latter work, no structural constraints nor bias potentials were employed, very long simulations had to be carried out to observe the formation of post-critical nuclei and the subsequent crystallization of the models. Metadynamics has enabled us to overcome this problem. In principle, this method also allows one to reconstruct the exact (coarse-grained) free energy surface of the system.[40] Nevertheless, long simulations are generally required to obtain converged values of this quantity. This fact, together with the need to use large models to describe crystallization processes, makes it challenging to determine the free energy barrier for nucleation using ab initio methods.

Our computed growth velocities are compatible with experimental estimates obtained from ultrafast differential scanning calorimetry measurements of the as-deposited amorphous state.[4] In another study,[6] the growth velocity of melt-quenched, doped GST was measured in the temperature range between 353 K and 543 K, using phase-change memory cells.[6] From their measurements, a velocity of about 0.1 m s^{-1} was extrapolated for T = 600 K. This value is smaller than the one yielded by our simulations. However, the extrapolated value depends sensitively on the parameters and the type of model used (due to the fragile behavior of GST, the growth velocity does not follow the Arrhenius law). Furthermore, doping can significantly alter the crystallization properties of PCMs . Although the nature of the dopant is not mentioned in the paper, doping of GST is usually done to further stabilize the amorphous state at low temperature, and typically results in slower crystallization at high temperature.[41,42] Finally, we should mention that finite size effects could lead to an overestimation of the growth velocity in our simulations. We believe this effect is rather small. Nevertheless, this point deserves further investigation.

In conclusion, our AIMD simulations have enabled us to compute the high temperature (600 K) growth velocity of GST adequately and efficiently. We have circumvented the (computationally demanding) problem of simulating the stochastic processes of nucleation by a) using the metadynamics method to accelerate the formation of sizable nuclei and b) considering amorphous models inside a crystalline matrix, so that crystallization occurs via growth from the interface. The growth velocities obtained, of the order of 1 m s^{-1}, are in fair agreement with previous experimental work. Our simulations also provide evidence that, upon fast crystallization from the amorphous phase on a subnanosecond time scale, a disordered cubic phase is formed, in which the distribution of vacancies, Ge and Sb atoms appears to be uncorrelated.

Supporting Information

Supporting Information is available from the Wiley Online Library or from the author.

Acknowledgements

The authors thank M. Wuttig, S. Caravati, G. C. Sosso, M. Bernasconi, and M. Parrinello for useful discussions. I.R. acknowledges warm hospitality during his visit at the Università della Svizzera Italiana. The authors also acknowledge the computational resources granted by JARA-HPC from RWTH Aachen University under project JARA0046, as well as funding by the DFG (German Science Foundation) within the collaborative research centre SFB 917 "Nanoswitches."

Received: March 3, 2015
Revised: April 8, 2015
Published online: May 5, 2015

[1] S. R. Ovshinsky, *Phys. Rev. Lett.* **1968**, *21*, 1450.
[2] M. Wuttig, N. Yamada, *Nat. Mater.* **2007**, *6*, 824.
[3] S. Raoux, W. Welnic, D. Ielmini, *Chem. Rev.* **2010**, *110*, 240.
[4] J. Orava, A. L. Greer, B. Gholipour, D. W. Hewak, C. E. Smith, *Nat. Mater.* **2012**, *11*, 279.
[5] M. Salinga, E. Carria, A. Kaldenbach, M. Bornhöfft, J. Benke, J. Mayer, M. Wuttig, *Nat. Commun.* **2013**, *4*, 2371.
[6] A. Sebastian, M. Le Gallo, D. Krebs, *Nat. Commun.* **2014**, *5*, 4314.
[7] R. Jeyasingh, S. W. Fong, J. Lee, Z. Li, K.-W. Chang, D. Mantegazza, M. Asheghi, K. E. Goodson, H.-S. Philip Wong, *Nano Lett.* **2014**, *14*, 3419.
[8] G. C. Sosso, J. Behler, M. Bernasconi, *Phys. Status Solidi B* **2012**, *10*, 1880.
[9] G. C. Sosso, G. Miceli, S. Caravati, F. Giberti, J. Behler, M. Bernasconi, *J. Phys. Chem. Lett.* **2013**, *4*, 4241.
[10] W. Zhang, I. Ronneberger, M. Xu, M. Salinga, M. Wuttig, R. Mazzarello, *Sci. Rep.* **2014**, *4*, 6529.
[11] K. Shportko, S. Kremers, M. Woda, D. Lencer, J. Robertson, M. Wuttig, *Nat. Mater.* **2008**, *7*, 653.

© 2015 WILEY-VCH Verlag GmbH & Co. KGaA, Weinheim

[12] D. Lencer, M. Salinga, B. Grabowksi, T. Hickel, J. Neugebauer, M. Wuttig, *Nat. Mater.* **2008**, *7*, 972.
[13] A. V. Kolobov, P. Fons, A. I. Frenkel, A. L. Ankudinov, J. Tominaga, T. Uruga, *Nat. Mater.* **2004**, *3*, 703.
[14] D. A. Baker, M. A. Paesler, G. Lucovsky, S. C. Agarwal, P. C. Taylor, *Phys. Rev. Lett.* **2006**, *96*, 255501.
[15] S. Kohara, K. Kato, S. Kimura, H. Tanaka, T. Usuki, K. Suzuya, H. Tanaka, Y. Moritomo, T. Matsunaga, N. Yamada, Y. Tanaka, H. Suematsu, M. Takata, *Appl. Phys. Lett.* **2006**, *89*, 201910.
[16] A. Klein, H. Dieker, B. Späth, P. Fons, A. Kolobov, C. Steimer, M. Wuttig, *Phys. Rev. Lett.* **2008**, *100*, 016402.
[17] S. Caravati, M. Bernasconi, T. D. Kühne, M. Krack, M. Parrinello, *Appl. Phys. Lett.* **2007**, *91*, 171906.
[18] J. Akola, R. O. Jones, *Phys. Rev. B: Condens. Matter* **2007**, *76*, 235201; *Phys. Rev. Lett.* **2008**, *100*, 205502.
[19] R. Mazzarello, S. Caravati, S. Angioletti-Uberti, M. Bernasconi, M. Parrinello, *Phys. Rev. Lett.* **2010**, *104*, 085503.
[20] G. C. Sosso, S. Caravati, R. Mazzarello, M. Bernasconi, *Phys. Rev. B: Condens. Matter* **2011**, *83*, 134201.
[21] S. Caravati, D. Colleoni, R. Mazzarello, T. D. Kühne, M. Krack, M. Bernasconi, M. Parrinello, *J. Phys.: Condens. Matter* **2011**, *23*, 265801.
[22] J. Hegedüs, S. R. Elliott, *Nat. Mater.* **2008**, *7*, 399.
[23] T. H. Lee, S. R. Elliott, *Phys. Rev. Lett.* **2011**, *107*, 145702.
[24] T. H. Lee, S. R. Elliott, *Phys. Rev. B: Condens. Matter* **2011**, *84*, 094124.
[25] J. Kalikka, J. Akola, J. Larrucea, R. O. Jones, *Phys. Rev. B: Condens. Matter* **2012**, *86*, 144113.
[26] J. Kalikka, J. Akola, R. O. Jones, *Phys. Rev. B: Condens. Matter* **2014**, *90*, 184109.
[27] B. J. Kooi, T. M. J. De Hosson, *J. Appl. Phys.* **2002**, *92*, 3584.
[28] T. Siegrist, P. Jost, H. Volker, M. Woda, P. Merkelbach, C. Schlockermann, M. Wuttig, *Nat. Mater.* **2011**, *10*, 202.
[29] W. Zhang, A. Thiess, P. Zalden, R. Zeller, P. H. Dederichs, J.-Y. Raty, M. Wuttig, S. Blügel, R. Mazzarello, *Nat. Mater.* **2012**, *11*, 952.
[30] A. Laio, M. Parrinello, *Proc. Natl. Acad. Sci. USA* **2002**, *99*, 12562.
[31] T. D. Kühne, M. Krack, F. R. Mohamed, M. Parrinello, *Phys. Rev. Lett.* **2007**, *98*, 066401.
[32] J. VandeVondele, M. Krack, F. Mohamed, M. Parrinello, T. Chassaing, J. Hutter, *Comput. Phys. Commun.* **2005**, *167*, 103; www.cp2k.org.
[33] J. P. Perdew, K. Burke, M. Ernzerhof, *Phys. Rev. Lett.* **1996**, *77*, 3865.
[34] S. Goedecker, M. Teter, J. Hutter, *Phys. Rev. B: Condens. Matter* **1996**, *54*, 1703.
[35] P. R. ten Wolde, M. J. Ruiz-Montero, D. Frenkel, *Faraday Discuss.* **1996**, *104*, 93.
[36] D. Quigley, P. M. Rodger, *Mol. Simul.* **2009**, *35*, 613.
[37] C. H. Rycroft, *Chaos* **2009**, *27*, 041111.
[38] R. De Bastiani, E. Carria, S. Gibilisco, A. Mio, C. Bongiorno, F. Piccinelli, M. Bettinelli, A. R. Pennisi, M. G. Grimaldi, E. Rimini, *J. Appl. Phys.* **2010**, *107*, 113521.
[39] N. N. Medvedev, V. P. Voloshin, V. A. Luchnikov, M. L. Gvrilova, *J. Comput. Chem.* **2006**, *27*, 1676; http://www.kinetics.nsc.ru/mds/?Software:VNP.
[40] G. Bussi, A. Laio, M. Parrinello, *Phys. Rev. Lett.* **2006**, *96*, 090601.
[41] R. M. Shelby, S. Raoux, *J. Appl. Phys.* **2009**, *105*, 104902.
[42] L. van Pieterson, M. H. R. Lankhorst, M. van Schijndel, A. E. T. Kuiper, J. H. J. Roosen, *J. Appl. Phys.* **2005**, *97*, 083520.

© 2015 WILEY-VCH Verlag GmbH & Co. KGaA, Weinheim